Spin-bus concept of spin quantum computing

Michael Mehring* and Jens Mende

2. Physikalisches Institut, University of Stuttgart, Germany

(Received 2 December 2005; published 4 May 2006)

We present a spin-bus concept of quantum computing where an electron spin $S=1/2$ acts as a *bus* qubit connected to a finite number N of nuclear spins $I=1/2$ serving as *client* qubits. Spin-bus clusters are considered as local processing units and may be interconnected with other spin-bus clusters via electron-electron coupling in a scaled up version. Here we lay the ground for the basic functional unit with long qubit registers, provide the theory and experimental verification of correlated qubit states, and demonstrate the Deutsch algorithm. Experiments were performed on a qubyte plus one nuclear spin in a solid state system.

I. INTRODUCTION

Experimental implementations of quantum algorithms by liquid state NMR [1] such as Deutsch's algorithm [2,3], Grover's quantum search algorithm [4,5], and Shor's algorithm [6] have dominated the experimental quantum computing scene since the beginning. Although the concept of pseudopure states [7,8] introduced in these implementations is conceptually rather appealing it was criticized because of the separability of the generated density matrices [9,10]. Interest has therefore been shifted more recently towards solid state devices which can be cooled to low temperatures and can reach the quantum limit. In this contribution we want to introduce a solid state concept of quantum computing where the topology can be viewed as a spin-bus system where a bus qubit, in our case labeled S-spin ($S=1/2$), couples to many I-spins ($I=1/2$) client qubits. We call this in the following the S-bus system. Since all client qubits are initially uncorrelated this resembles the interesting concept of the power of one bit of quantum information by Knill and Laflamme [11].

In Fig. 1 we have sketched the basic unit of an S-bus system which can be extended by interconnecting several units via couplings among the S-spins to create a network. This requires a controllable wave function delocalization among $S_1, \ldots, S_M$ bus qubits similar to the Kane proposal [12]. This might also be applicable to electron qubits in quantum dots [13–15]. In the following sections, however, we will restrict ourselves to the basic unit of an S-bus system as presented in the bottom part of Fig. 1. In addition the global coupling of the S-spin to all I-spins also local couplings among the I-spins by direct and indirect spin-spin interactions can be considered. In this concept the S-spin serves not only as the qubit which monitors the state of the I-spins but also allows one to correlate the I-spins among themselves as will be discussed in the following. Although we demonstrate the principle here for the case of $CaF_2:Ce^{3+}$ this concept could equally well be applied to $^{29}Si:P^+$ [16]. It is also not restricted to spins 1/2 but can be extended two any ensemble of two-level systems coupled to a central *bus* qubit.

*Electronic address: m.mehring@physik.uni-stuttgart.de

II. BASIC CONCEPTS

The general processing sequence of the S-bus system is displayed in Fig. 2. It begins with a preparation sequence consisting of unitary transformations applied to both the S-spin as well as a selected number of I-spins.

The general sequence of events when performing quantum algorithms within the S-bus concept is sketched in Fig. 2. First a preparations sequence, represented by the unitary transformation $U_P^{(S)}$, is applied only to the S-spin which results in a highly correlated state of the I-spin qubits as will be shown. This is followed by a sequence of unitary transformations U_I applied only to the qubit spins I_j which includes special initial density matrix preparations as well as implementing quantum algorithms followed by tomography and readout pulses with projection to the qubit eigenstates. All quantum algorithms applied to the *client* qubits lead at the end of the sequence of events to a state which is pro-
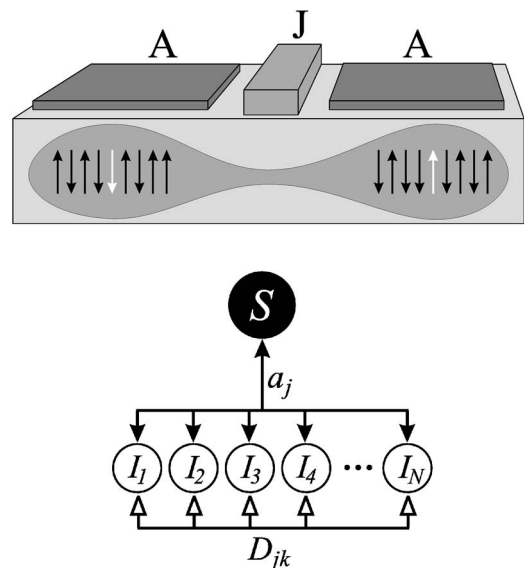
FIG. 1. Top: Sketch of a controllable S-bus system where the hyperfine interaction is controlled via A gates and the coupling between different S-bus systems is mediated via a J-gate [12]. Bottom: Basic unit of an S-bus system with *bus* qubit S and *client* qubits I_j.

FIG. 2. Sequence of events in an *S*-bus system with initial preparation ($U_P^{(S)}$) and detection ($U_D^{(S)}$) sequences applied to the *bus* spin *S*. Quantum algorithms are performed by the locally addressed *I*-spins. The unitary transformations U_I applied to the *I*-spins are embedded between appropriate state preparation and detection sequences. Final detection is performed by a remote echo detection (RED) sequence at the *S*-spins.

jected to a diagonal state by the detection sequence. This is monitored by a remote electron spin echo detection. We note that the *S*-bus system comprises two different nuclear qubit subsystems, namely, those coupled to electron spins in state $m_S=+1/2$ and $m_S=-1/2$. In the experiments to be discussed only one of these subsystems is selected.

A. Initial state preparation

We consider an electron spin $S=1/2$ coupled to many nuclear spins I_j by hyperfine interaction expressed by the Hamiltonian $H_{SI}=\Sigma_j^N a_j I_{zj} S_z$. For simplicity we restrict ourselves here to the secular components of the hyperfine tensor. The general case will be discussed elsewhere. No initial nuclear spin polarization is assumed, i.e., we start from an initial Boltzmann density matrix for *M* electron spins as

$$\rho_B = \prod_{j=1}^{M} \left(\frac{1}{2}I_2 - \Theta S_{zj} \right) \qquad (1)$$

with $\Theta=\tanh[\hbar\omega/(2k_BT)]$ and where I_2 is the 2×2 identity matrix. When expressed as a series expansion Eq. (1) contains S_{zj} spin operator products of power *m* with prefactors Θ^m representing Boltzmann correlations of the *S* spins. In this contribution we restrict ourselves to the low field, high temperature approach resulting in

$$\rho_B = \frac{1}{2}I_2 - \Theta S_z \qquad (2)$$

which is valid for $\Theta \ll 1$. Since no initial *I*-spin polarizations or correlations are assumed these have to be created through the hyperfine interaction with the electron spins as will be shown in the following leading to an initial density matrix after preparation as

$$\rho_P = \frac{1}{2^{N+1}}I_{N+1} - \Theta S_z \otimes \rho_I, \qquad (3)$$

where ρ_I represents a highly correlated state of the *N* *I*-spin qubits and where I_{N+1} is the $(N+1)\times(N+1)$ identity matrix. All experiments start with a $P_y(\pi/2)$ pulse applied to the

Boltzmann density matrix followed by some free evolution for time τ_S under the hyperfine Hamiltonian H_{SI} which leads to the initial density matrix

$$\rho_{\text{ini}} = \frac{1}{2^{N+1}}I_{N+1} - \Theta\frac{1}{2}(\Pi_N^{(-)}S_+ + \Pi_N^{(+)}S_-), \qquad (4)$$

where we use the shorthand notation

$$\Pi_N^{(\pm)} = \prod_{j=1}^{N} e^{\pm i\tau_S a_j I_{zj}}. \qquad (5)$$

This reduces for qubits ($I=1/2$) to

$$\Pi_N^{(\pm)} = \prod_{j=1}^{N} (c_j I_2 \pm 2is_j I_{zj}), \qquad (6)$$

where we have used the abbreviations $c_j=\cos(\tau a_j/2)$ and $s_j=\sin(\tau a_j/2)$ and I_2 for the 2×2 identity matrix.

The sequence leading to ρ_{ini} is complemented by another $\pi/2$ pulse which transfers the x,y components of the *S*-spin to z. After an appropriate waiting time all leftover transverse components have decayed by destructive interference. This leads in general to the operator part $\rho_{\text{prep}}=\rho_I S_z$ of the density matrix after preparation where here and in the following the product is a tensor product and ρ_I depends on the applied preparation sequence and its duration τ_S. See Appendix A for further details. In the following section we discuss a number of different basic preparation sequences. More elaborate sequences are possible and have been tested but are beyond the scope of this contribution.

B. Algorithms and readout

The initial preparation sequence is followed by the qubit algorithms including preparation steps, quantum algorithms, and a readout step as is sketched in Fig. 2. This leads in general to a change of the initial density matrix expressed by the tilde in $\tilde{\rho}_I$:

$$\tilde{\rho}_{IS} = \tilde{\rho}_I S_z. \qquad (7)$$

In order to transform $\tilde{\rho}_{IS}$ to an observable *S*-spin state a detection sequence, represented by the unitary transformation $U_D^{(S)}$, is applied solely to the *S*-spins followed by an electron spin echo sequence. This scenario leads to the following sequence of transformation:

$$|\rho_D) = U_D^{(S)} \cdots U_I \cdots U_P^{(S)}|S_z) = U_D^{(S)}\tilde{\rho}_I|S_z), \qquad (8)$$

where ρ_D represents the density matrix at detection time. Only the diagonal part of the density matrix ρ_D is considered for detection, that is, enough waiting time is included before the final electron spin echo sequence is applied to allow for the decay of all transverse components.

The general expression for the signal at detection time can be expressed as

$$S_D = \frac{(S_z|\rho_D)}{(S_z|S_z)} = \frac{(Q_D^{(S)}|U_I|Q_P^{(S)})}{(S_z|S_z)}, \tag{9}$$

where we have used in the second part the abbreviations $Q_D^{(S)} = U_D^{(S)} S_z U_D^{(S)\dagger}$ and $Q_P^{(S)} = U_P^{(S)} S_z U_P^{(S)\dagger}$. Often we will use $U_D^{(S)} = U_P^{(S)}$ which leads to $Q_D^{(S)} = Q_P^{(S)}$.

Note that there are two sets of N qubits, namely, those corresponding to electron spin states $m_S = \pm 1/2$. We therefore split the density matrix ρ_D according to Eq. (8) into

$$\rho_D = \rho_I \tilde{\rho}_I \frac{1}{2} \left(\frac{I_2}{2} + S_z \right) - \rho_I^2 \frac{1}{2} \left(\frac{I_2}{2} - S_z \right), \tag{10}$$

where we have assumed that qubit algorithms are performed only in the $m_S = +1/2$ subsystem. This leads to the detection signal

$$S_D = \frac{\text{Tr}\{S_z \rho_D\}}{\text{Tr}\{S_z^2\}} = \frac{1}{2} \left(\frac{\text{Tr}_I\{\rho_I \tilde{\rho}_I\}}{2^N} + \frac{\text{Tr}_I\{\rho_I^2\}}{2^N} \right), \tag{11}$$

where the first part contains the signal expression of the quantum algorithm (note the tilde) and the second part is an offset term not affected by the quantum algorithm. In the following sections we will focus on the first part.

III. PREPARATION OF LONG QUBIT REGISTERS

Starting from zero I-spin correlations the S-bus topology allows one to introduce spin-spin correlations among the I-spins by applying specific unitary transformations only to the S-spin. Different simple pulse sequences will be discussed in the following which create specific I-spin correlations.

A. The yy sequence

This sequence consists of two consecutive $P_y^{(S)}(\pi/2)$ pulses applied to the electron spin separated by a time τ_S. The pair of pulses is typically applied in the stimulated echo sequence and has been proposed by Mims for his pulsed ENDOR version (Mims ENDOR) [17]. This leads according to Eqs. (3) and (A3) to the following density matrix for the yy-preparation sequence:

$$Q_P^{(yy)} = \frac{1}{2^{N+1}} I_{N+1} - \Theta S_z \otimes \rho_{yy} \tag{12}$$

with I-spin density matrix

$$\rho_{yy} = \text{Re} \left(\prod_{j=1}^{N} (c_j I_2 + i s_j 2 I_{zj}) \right) \tag{13}$$

for N qubits ($I=1/2$) and where $c_j = \cos(\tau_S a_j/2)$ and $s_j = \sin(\tau_S a_j/2)$. When the product is expanded the high order nuclear spin operator products, i.e., qubit correlations show up as will be shown below. Note that these correlations build up (with no irradiation performed at the I-spins) during the preparation sequence of duration τ_S which is for the system discussed here typically on the order of $20-100$ ns depending on the strength of the hyperfine interaction.

The high degree of nuclear spin correlations becomes immediately apparent when expanding the product in Eq. (13) for the special case of $N=4$ which leads to

$$\begin{aligned}
\rho_{yy} = {} & c_1 c_2 c_3 c_4 I_4 - 2^2 (I_{z1} I_{z2} s_1 s_2 c_3 c_4 + I_{z1} I_{z3} s_1 s_3 c_2 c_4 \\
& + I_{z1} I_{z4} s_1 s_4 c_2 c_3 + I_{z2} I_{z3} s_2 s_3 c_1 c_4 + I_{z2} I_{z4} s_2 s_4 c_1 c_3 \\
& + I_{z3} I_{z4} s_3 s_4 c_1 c_2) + 2^4 (I_{z1} I_{z2} I_{z3} I_{z4} s_1 s_2 s_3 s_4),
\end{aligned} \tag{14}$$

where I_4 is the identity matrix appropriate for the number of qubits here and which will be in general a $2^N \times 2^N$ identity matrix. The number of elements with k fold products of spin operators are given by the binomial coefficient

$$\binom{N}{k} = \frac{N!}{(k)!(N-k)!}. \tag{15}$$

Accordingly we expect for $N=4$ a total number of $\binom{4}{2}=6$ two spin correlations and $\binom{4}{4}=1$ four spin correlation. Note that ρ_{yy} can be expressed as a sum of only even products of spin operators up to the maximum N. The prefactors are given by the sine and cosine functions of $\tau_S a_j/2$. They can be tuned by choosing the appropriate value of the pulse separation τ_S for a given set of hyperfine parameters a_j.

B. The yx sequence

If we replace the second y-pulse in the two pulse sequence of the previous section by an x pulse, we obtain the preparation operator

$$Q_P^{(yx)} = \frac{1}{2^{N+1}} I_{N+1} - \Theta S_z \otimes \rho_{yx} \tag{16}$$

with

$$\rho_{yx} = -\text{Im} \left(\prod_{j=1}^{N} (c_j I_2 + i s_j 2 I_{zj}) \right). \tag{17}$$

As in the case of the yy sequence we obtain the nuclear spin correlations produced after the yx sequence by expanding the product in Eq. (17) for $N=4$ as

$$\begin{aligned}
\rho_{yx} = {} & -2 (I_{z1} s_1 c_2 c_3 c_4 + I_{z2} s_2 c_1 c_3 c_4 + I_{z3} s_3 c_1 c_2 c_4 + I_{z4} s_4 c_1 c_2 c_3) \\
& + 2^3 (I_{z1} I_{z2} I_{z3} s_1 s_2 s_3 c_4 + I_{z1} I_{z2} I_{z4} s_1 s_2 s_4 c_3 \\
& + I_{z1} I_{z3} I_{z4} s_1 s_3 s_4 c_2 + I_{z2} I_{z3} I_{z4} s_2 s_3 s_4 c_1).
\end{aligned} \tag{18}$$

Note that ρ_{yx} can be expressed as a sum of odd order products of spin operators up to the maximum of N for odd N and of $(N-1)$-fold products for even N.

C. The $y\pi4$ sequence

If we phase shift the second y-pulse in the Mims sequence by $-\pi/4$ we obtain the preparation operator

$$Q_P^{(y\pi4)} = \frac{1}{2} I_0 - \Theta S_z \otimes \rho_{y\pi4} \tag{19}$$

with

$$\rho_{y\pi4} = \frac{1+i}{2\sqrt{2}}\prod_{j=1}^{N}(c_j I_2 + i s_j 2 I_{zj}) + \frac{1-i}{2\sqrt{2}}\prod_{j=1}^{N}(c_j I_2 - i s_j 2 I_{zj})$$

$$(20)$$

which can be reformulated in terms of the previous density matrices as

$$\rho_{y\pi4} = \frac{1}{\sqrt{2}}(\rho_{yy} + \rho_{yx}). \qquad (21)$$

Note that this sequence combines the even and odd numbered correlations of nuclear spins of the yy and yx sequences. Similar results can be obtained if the second pulse in the yy sequence is replaced by a $\pi/4x$ pulse followed immediately by a $\pi/4y$ pulse. This avoids unconventional phase shifting but leads to different prefactors for odd and even correlated qubit expressions.

As an example we expand the case of $N=3$ which results in

$$\rho_{y\pi4} = \frac{1}{\sqrt{2}}[c_1 c_2 c_3 I_3 - 2(I_{z1} s_1 c_2 c_3 + I_{z2} s_2 c_1 c_3 + I_{z3} s_3 c_1 c_2)$$

$$+ 2^2(I_{z1} I_{z2} s_1 s_2 c_3 + I_{z1} I_{z3} s_1 s_3 c_2 + I_{z2} I_{z3} s_2 s_3 c_1)$$

$$- 2^3 I_{z1} I_{z2} I_{z3} s_1 s_2 s_3]. \qquad (22)$$

We note that for $c_j = s_j = 1/\sqrt{2}$ Eq. (22) leads to $\rho_{y\pi4} = 2\rho_{111}$ where ρ_{111} is a three qubit pure state. This is true, however, only for the subspace of qubits.

IV. SIGNAL DETECTION

If the detection sequence equals the preparation sequence the relevant detected signal can according to Eq. (11) in general be expressed as

$$S_D = \frac{1}{2^N}\mathrm{Tr}\{\rho_I \tilde{\rho}_I\}, \qquad (23)$$

where $\tilde{\rho}_I = U_I \rho_I U_I^\dagger$ corresponds to the transformation of ρ_I by the quantum algorithm U_I. Equation (23) covers the signal response due to any type of quantum algorithm applied to the nuclear spins. All qubit algorithms are set up in such a way that at the detection point only diagonal states are present which allows to express the outcome by a scaling factor $-1 \leq S_j \leq 1$ in front of every I_{zj} operators which has been addressed. This basically involves replacing every s_j parameter in ρ_i by $s_j \rightarrow s_j S_j$. Special cases involving reordering qubits need to be treated separately.

In Appendix A the general case of long qubit registers of size N is discussed, where only a subset of n qubits takes part in the quantum algorithm. Applying Eq. (23) to these long registers leads for the different preparation sequences to the following detection signals:

$$S_{yy} = \frac{1}{2}\left(\prod_{j=1}^{n}(c_j^2 + s_j^2 S_j) + M_{N-n}\prod_{j=1}^{n}(c_j^2 - s_j^2 S_j)\right), \quad (24a)$$

$$S_{yx} = \frac{1}{2}\left(\prod_{j=1}^{n}(c_j^2 + s_j^2 S_j) - M_{N-n}\prod_{j=1}^{n}(c_j^2 - s_j^2 S_j)\right), \quad (24b)$$
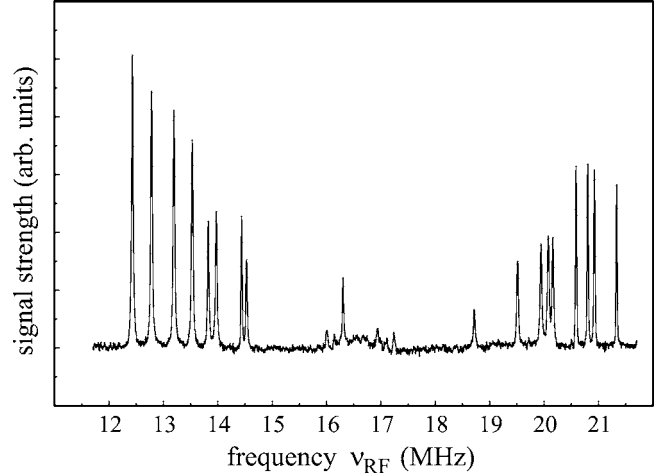
FIG. 3. ENDOR spectrum of the qubyte plus one system CaF_2:Ce with all $2\cdot9=18$ hyperfine lines of the nine ^{19}F resolved.

$$S_{y\pi4} = \frac{1}{2}\prod_{j=1}^{n}(c_j^2 + s_j^2 S_j), \qquad (24c)$$

where

$$M_{N-n} = \prod_{k=n+1}^{N}(c_k^2 - s_k^2). \qquad (25)$$

with $M_0 = 1$ for $(n=N)$. In the following we will also often use the parameters

$$P_n^{(\pm)} = \frac{1}{2}(1 \pm M_{N-n}). \qquad (26)$$

V. TOMOGRAPHY OF I-SPIN CORRELATIONS

Before we proceed to the implementation of the Deutsch algorithm within the S-bus concept, we treat the preparation of pseudopure initial states and their tomography by pulsed electron nuclear double resonance (ENDOR) and multiple quantum ENDOR (MQE). This technique was first introduced in ENDOR in order to measure proton-proton nuclear spin correlations [18]. See also the earlier work on hetero nuclear multiple quantum NMR [19–22] and a more recent contribution [23].

A. Selective nuclear spin excitations

In order to address the nuclear spins individually we need to have a system with well separated hyperfine lines. Our working horse which will be discussed in more detail in a separate contribution is CaF_2:Ce^{3+} which provides us with a qubyte plus one ^{19}F nuclear spins $1/2$ as can be seen from the ENDOR spectrum shown in Fig. 3 [24,25]. This spectrum was obtained by applying a single π-pulse with varying frequency over the full spectral width. All experiments reported in this contribution were performed at the X band (9.5 GHz) at around 10 K. Here and in the following we express, except when noted otherwise, the effect of a selec-

tive β_j-pulse applied to a spin I_j by the scaling of its z component resulting in $I_{zj} \rightarrow \cos \beta_j I_{zj} = S_j I_{zj}$. For detection we assume that transient x, y components of the magnetization have decayed after the pulse. In other words a prefactor $S_j \leqslant 1$ is attached to all addressed spins I_j in the density matrix. The maximum effect is achieved for a π pulse.

The general ENDOR signal can be defined by applying Eqs. (24a) and (26) with $n = 1$:

$$S_{yy} = c_j^2 P_1^{(+)} + s_j^2 P_1^{(-)}. \qquad (27)$$

If we define the ENDOR signal as the difference between the signal with no irradiation applied at spin I_j ($S_j = 1$) and with irradiation represented by an arbitrary value of S_j obeying the condition $-1 \leqslant S_j \leqslant 1$ we obtain

$$S_{\text{ENDOR}} = (1 - S_j) s_j^2 P_1^{(-)}. \qquad (28)$$

The maximum ENDOR effect is achieved with a π-pulse which inverts the nuclear spin ($S_j = -1$) leading to

$$S_{\text{ENDOR}}^{(\text{max})} = \sin\left(\tau \frac{a_j}{2}\right)^2 \left(1 - \prod_{k \neq j}^{N} \cos(\tau a_k)\right). \qquad (29)$$

We note that the ENDOR signal intensity of an individual line depends on all the residual hyperfine interactions. However, small hyperfine interactions which obey the relation $\tau a_k \ll 1$ do not contribute significantly. This can be controlled by the appropriate choice of τ_S (hyperfine filter)(see center part of Fig. 3).

B. Multiple quantum ENDOR tomography

The ENDOR spectrum provides no information on the nuclear spin correlations. In order to determine these we use multiple quantum ENDOR (MQE) [18]. The corresponding sequence is shown in Fig. 4.

It utilizes the selective phase encoding of each individual spin I_j with individual phase φ_j. This allows one to separate different multiple-quantum coherences as was shown by Drobny *et al.* [19] and Bodenhausen *et al.* [26] in NMR. To be more concrete we consider the simple case of two qubits, i.e., we select two ENDOR lines out of the set of lines. A typical example of the results to be expected for two qubits is shown in Fig. 4 (bottom). We note that the four lines relate to so-called 0Q (zero-quantum), 1Q (one-quantum), and 2Q (two-quantum) lines which will be explained in the following section.

1. Two qubit MQE

The initial density matrix can be expressed according to Eq. (A18) as

$$\rho_I^{(2)} = \frac{1}{2^2} p_0 I_2 + \frac{1}{2} p_1 I_{z1} + \frac{1}{2} p_2 I_{z2} + p_{12} I_{z1} I_{z2}, \qquad (30)$$

where the p_1, p_2, and p_{12} variables depend on the hyperfine interactions and the pulse spacing τ_S of the preparation sequence. We will see later how these variables can be tuned to $p_1 = p_2 = p_{12} = 1$ which would convert $\rho_y^{(2)}$ into the pseudopure density matrix ρ_{00} of a two qubit system.
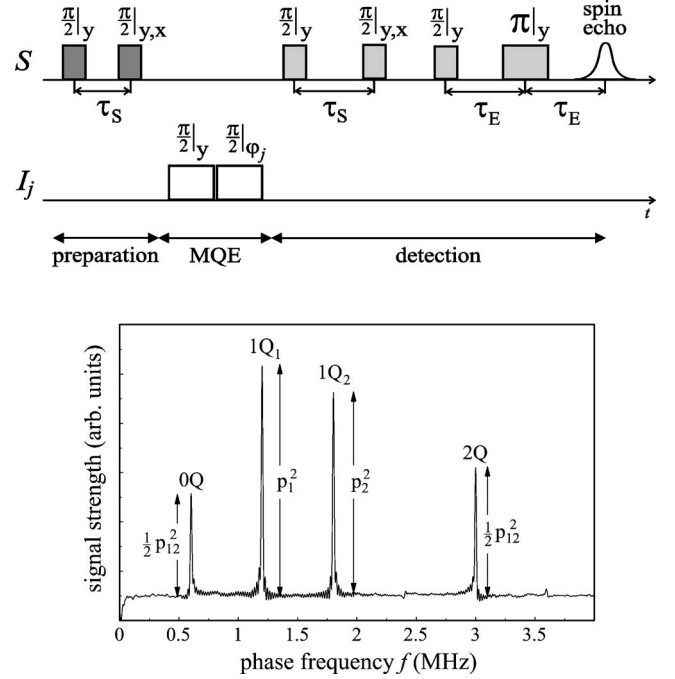
FIG. 4. Top: Pulse sequence for performing MQE experiments. Bottom: Typical MQE spectrum obtained for a two qubit system (see text).

After application of the two-pulse MQE sequence $P_{xj}(-\pi/2, \varphi_j) P_{xj}(\pi/2, 0)$ to spins $j \in \{1, 2\}$ and where the phase φ_j is defined in the rotating frame with reference to the x direction the density matrix is converted to

$$\tilde{\rho}_I^{(2)} = \frac{1}{2} p_1 \cos \varphi_1 I_{z1} + \frac{1}{2} p_2 \cos \varphi_2 I_{z2} + p_{12} \cos \varphi_1 \cos \varphi_2 I_{z1} I_{z2}$$

$$(31)$$

after all transient components have decayed. This leads to the MQE signal

$$S_D = \text{Tr}\{\rho_I^{(2)} \tilde{\rho}_I^{(2)}\} = \frac{1}{4}(p_0^2 + p_1^2 \cos \varphi_1 + p_2^2 \cos \varphi_2$$

$$+ p_{12}^2 \cos \varphi_1 \cos \varphi_2) \qquad (32)$$

which can be represented as a phase interferogram. Phase shifting of the pulse sequence can be performed in increments according to $\varphi_j = 2\pi f_j t$ which introduces a virtual time t [19,26]. After Fourier transformation (FT) this results in a spectrum with the four frequencies and amplitudes as given in Table I.

TABLE I. The four frequencies and amplitudes (except for a constant factor) of a two spin MQE spectrum.

Freq.	$f_1 - f_2$	f_1	f_2	$f_1 + f_2$
Ampl.	$\frac{1}{2} p_{12}^2$	p_1^2	p_2^2	$\frac{1}{2} p_{12}^2$

TABLE II. The four frequencies and amplitudes (except for a constant factor) of a two spin MQE spectrum.

p_0	p_1	p_2	p_{12}
$c_1^2 c_2^2 P_2^{(+)}$	$s_1^2 c_2^2 P_2^{(-)}$	$s_2^2 c_1^2 P_2^{(-)}$	$s_1^2 s_2^2 P_2^{(+)}$

In summary phase interferometry can be used to distinguish the different nuclear spin correlations and determine their contribution to the density matrix (density matrix tomography). We will show in Sec. VI that the same sequences can also be used to tune the prefactors and prepare pseudopure density matrices.

2. Multiple qubit MQE

In the previous section we have treated the most simple case of two spins as an introductory example. This is, however, unrealistic because there are usually many more nuclei coupled to an electron spin. We extend therefore the scenario to the realistic case where many nuclei $\{N\}$ are coupled to an electron spin but only a subset of $\{n\}$ nuclei is addressed. Here we apply the generalizations derived in Appendix A and Eq. (24).

When replacing S_j by $\cos \varphi_j$ we obtain

$$S_{\text{MQE}} = \frac{1}{2} \prod_{j \in \{n\}} (c_j^2 + \cos \varphi_j s_j^2) + \frac{1}{2} M_{N-n} \prod_{j \in \{n\}} (c_j^2 - \cos \varphi_j s_j^2).$$
(33)

Individual variation of the local phase factors leads after Fourier transform to the MQE spectrum. From this the correlation factors can be determined as was discussed for the two qubit case in the previous section.

Applying this to two qubit case leads to

$$S_{\text{MQE}} = c_1^2 c_2^2 P_2^{(+)} + (\cos \varphi_1 s_1^2 c_2^2 + \cos \varphi_2 s_2^2 c_1^2) P_2^{(-)}$$
$$+ \cos \varphi_1 \cos \varphi_2 s_1^2 s_2^2 P_2^{(+)}.$$
(34)

Comparing Eq. (32) with Eq. (34) allows us to identify the square of the prefactors of the two qubit density matrix with the correlation parameters as shown Table II except for an overall factor of 2^2.

The extension to more qubits is straightforward and will be discussed in a separate contribution (see also Ref. [25,27]). Note that MQE spectra are only observed if correlations between the different qubits exist. This is not the case for qubits belonging to different $m_s \pm 1/2$ subsets. In this case only single quantum lines are visible in the MQE spectrum.

3. Nonselective MQE

If a large number of qubits are correlated the number of lines in the MQE spectrum increases exponentially. In order to demonstrate that a rather high degree of nuclear spin correlations can indeed be obtained by the standard *yy*-preparation sequence we present in Fig. 5 the nonselective MQE spectrum of the central part of the ENDOR spectrum (distant nuclei) by applying strong electron $\pi/2$ pulses and using the same phase incrementing frequency f for all nulei.
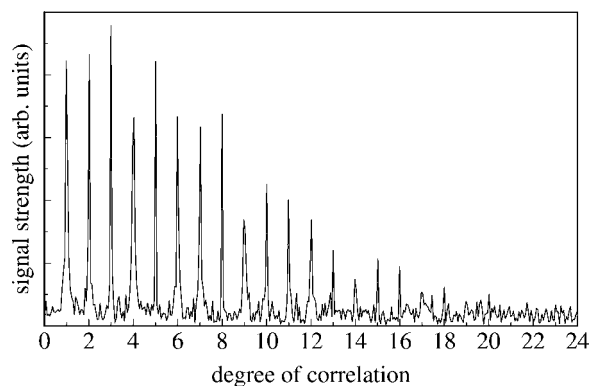
FIG. 5. MQE spectrum with the same phase incrementation frequency applied to nuclei in the center of the ENDOR spectrum (distant nuclei). The large pulse separation $\tau_S = 1.36 \ \mu s$ allows for the buildup of high order spin correlations. Up to twenty are seen.

The scenario for detecting high spin correlations as demonstrated for two spins in the previous sections can readily be extended to an arbitrary number of spins. The number of spectral lines increases, of course, exponentially. Here we demonstrate that a high degree of correlation can in fact be obtained as is demonstrated in Fig. 5 which displays the MQE spectrum with identical phase frequencies and excitation in the center part of the ENDOR spectrum (distant nuclei). Since the number of correlated spins depends on the τa_j product, it is obvious that longer preparation times should increase the number of correlated spins. Naturally the amplitude of higher correlations falls off rapidly as given by the binomial coefficient according to Eq. (15) (see also Refs. [21,22]). Krojanski and Suter have recently demonstrated that long qubit registers show peculiar decoherence times depending on the degree of correlations [28].

VI. PSEUDOPURE DENSITY MATRICES

Although the preparation sequence already creates a high degree of nuclear spin correlations the prefactors in front of the different spin products depend, however, on the sine and cosine functions of different $\tau a_j/2$ products and it cannot be expected that all p_j will fulfill the pseudopure state requirement $|p_j| = 1$ in Eq. (A18). One can choose appropriate τ_S values to come close to a pure or pseudo pure initial density matrix, but some final adjustment will in general still be required. This can be achieved by modifying each spin component I_{zj} by a prefactor $S_j \to \cos \beta_j$ precisely in the same way as used for the MQE procedure with the difference that now fixed phase angles β_j are used and are adjusted to achieve a pure or pseudopure initial density matrix. This basically implies that in Eq. (33) each $\cos \varphi_j$ is replaced by $\cos \varphi_j \cos \beta_j$ if in addition MQE tomography is wanted.

This procedure is applied in the next sections to the case of two and three qubits. We have also extended this to longer qubit registers.

A. The two qubit case

By adjusting the parameters $\cos \beta_j$ appropriately all pseudopure density matrices of the two qubit system have
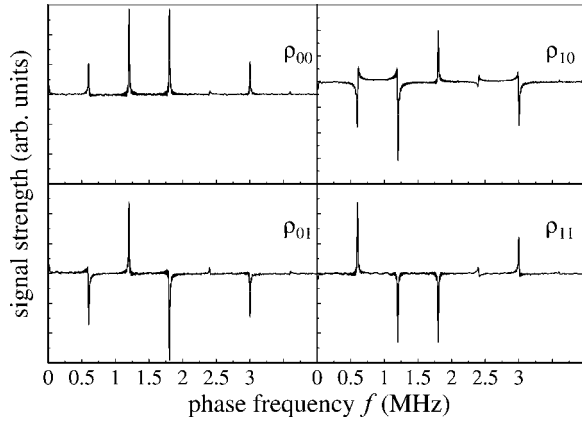
FIG. 6. MQE of the two qubit pseudopure density matrices after adjusting the prefactors S_1, S_2 appropriately to achieve $\rho_{00}, \rho_{01}, \rho_{10}, \rho_{11}$.

been obtained as is shown in Fig. 6. The initial density matrix is measured by MQE as described in Sec. V B by using the pulse sequence shown in Fig. 4. The two-pulse scaling sequence at the I-spin transitions is applied prior to the MQE sequence. There is a delay between these two pulse sequences of about 200 μs to let off-diagonal components decay. The parameters $|p_j|$ of the initial density matrix are determined by setting $\beta_j = 0$; $S_j = 1$ from the amplitudes of the MQE spectrum as outlined in Sec. V B. In the next step values of S_j are chosen according to Eq. (30) such that all $p_j = 1$ except for an overall constant factor. Note that the final MQE spectrum does not look like the pure state because of $\rho_I \neq \tilde{\rho}_I$ due to the two-pulse ESR detection sequence.

B. Three qubit density matrix

The preparation of three qubit pseudo-pure states is an extension of the procedure outlined in the case of two qubits by applying the corresponding pulse sequences selectively to the three qubits I_1, I_2, and I_3. Extensions to an arbitrary number of qubits is conceptually straightforward, however, experimentally more demanding.

In Fig. 7 we present the MQE spectrum of the as prepared density matrix (top) to be compared with the ρ_{000} state (bottom). Note that only minor adjustments were required because the as prepared density matrix was already very near ρ_{000}. The following phase incrementation frequencies were applied: $f_1 = 0.81$ MHz, $f_2 = 1.03$ MHz, and $f_1 = 1.16$ MHz. This results in spectral lines at frequencies $0Q$: $|f_j - f_k|$; $1Q$: f_j and $|f_j + f_k - f_q|$; $2Q$: $|f_j + f_k|$; $3Q$: $f_1 + f_2 + f_3$.

VII. CONTROLLED NOT OPERATION

The controlled NOT operation (CNOT) is one the of universal quantum gates which is the basis for many quantum algorithms. Its implementation within the S-bus system requires a spin-spin interaction between the control and target qubit. Here we use the direct and indirect dipole-dipole interaction between the nuclear spins.

If we express the interaction Hamiltonian of the two qubits as $H_{12} = D I_{z1} I_{z2}$ the free evolution period given by the
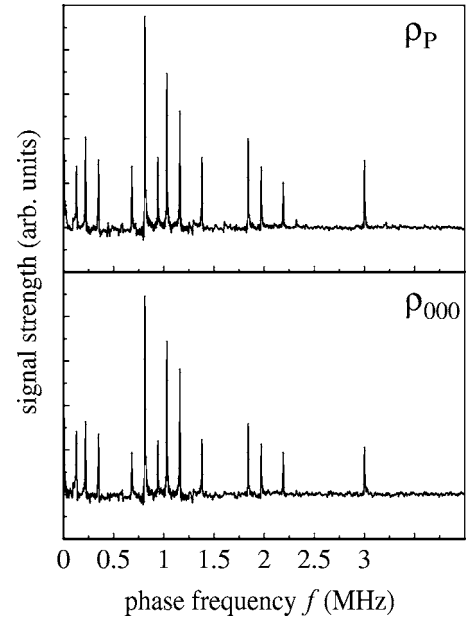
FIG. 7. MQE of the three qubit initial density matrix (top) and after adjusting the prefactors S_1, S_2, S_3 to achieve ρ_{000}. Only minimal adjustments were required.

unitary transformation $U_{12}(t) = \exp(-it H_{12})$ is complemented by the appropriate initial and final pulses (INEPT sequence [29] plus z rotations) to implement the CNOT gate. Our S-bus implementation is shown in Fig. 8. We note that the expected sinusoidal evolution with frequency $D_{12}/2$ is only observed if a yy preparation and a yx detection sequence is used. Alternatively one could apply a $y\pi4$ sequence both for preparation and detection. The CNOT operation is achieved by choosing the special value of $\tau = \pi/D_{12}$. This has been verified by density matrix tomography.

VIII. TWO QUBIT DEUTSCH ALGORITHM

According to the general scheme of the S-bus sequence the unitary transformations corresponding to quantum algorithms are embedded between the preparation and the detection sequence followed by the electron spin echo monitor sequence. They consist of arbitrary complex pulse sequences applied to spins I_j with $j \in \{1, \ldots, N\}$ out of the manifold N.

The Deutsch-Jozsa algorithm was one of the first quantum algorithms implemented with nuclear spins in liquid state NMR [2,3,30–32]. In the following, we briefly summarize the concepts of the Deutsch-Jozsa algorithm. The Deutsch-Jozsa problem [33] considers a set of functions which map a binary string of length N to a single bit:

$$f: \mathbb{Z}_{2^N} \mapsto \mathbb{Z}_2. \tag{35}$$

This requires a physical device which when given an input x will produce the corresponding output $f(x)$ of an *a priori* unknown function f from the set defined in Eq. (35). The task consists of answering the question whether the function f has any of the two properties: (i) it is constant or (ii) it is balanced, meaning that applied to all possible inputs
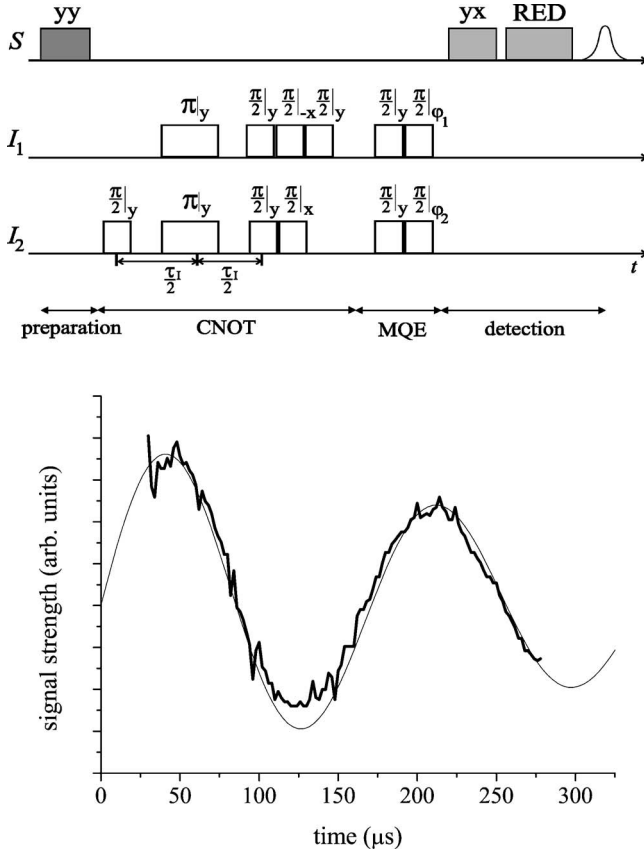
FIG. 8. Top: Pulse sequence for the implementation of the CNOT operation. Bottom: Evolution under the CNOT sequence for variation of τ_I. Solid line: Decaying sinosoid (see text).

it returns 0 exactly as often as 1. Deutsch and Jozsa have shown that a quantum computer can solve this problem exponentially faster than a classical computer.

A. The Collins version

The original version of the algorithm required $N+1$ qubits for a N-bit function and two evaluation steps. Later, Cleve, Ekert, Macchiavello, and Mosca (CEMM) modified the Deutsch-Jozsa (DJ) algorithm by reducing the number of evaluations to one [34]. Collins, Kim, and Holton removed the requirement of an ancilla qubit [35]. We used this optimized version of the DJ algorithm for the work reported here.

The block diagram for this extended version of the algorithm is shown in Fig. 9. We start with the initial state $|0\rangle_N$ with all N qubits in state $|0\rangle$. The DJ algorithm proceeds via the application of a Hadamard transformation $H_N = H \otimes H \otimes \cdots \otimes H \otimes H$ to put all N qubits in superposition followed by the unitary transformation U_f representing the unknown function $f(x)$. The decision on the class of the test function is

$$|X\rangle_{\text{in}} \multimap \boxed{H_j} \multimap \boxed{U_f} \multimap \boxed{H_j} \multimap |X\rangle_{\text{out}}$$
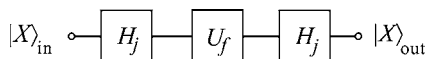
FIG. 9. Block diagram of the extended version of the Deutsch-Jozsa algorithm for N qubits.

TABLE III. Two qubit Deutsch functions.

x	00	01	10	11	
f_{0000}	0	0	0	0	constant
f_{0101}	0	1	0	1	balanced
f_{0011}	0	0	1	1	balanced
f_{0110}	0	1	1	0	balanced

based upon the amplitude of the state $|0\rangle_N$ in the output state

$$P(|0\rangle_N) = \frac{1}{2^N} \left| \sum_{k=0}^{2^N-1} (-1)^{f(k)} \right| = \begin{cases} 1 & \text{if } f \text{ constant,} \\ 0 & \text{if } f \text{ balanced.} \end{cases}$$
(36)

Just for demonstration how this is implemented within the S-bus concepts we present in the following the simplest version, namely, the case $N=2$. In this case there are $2^{2N}=16$ functions $f(x)$ with $x \in \{00, 01, 10, 11\}$ in total. Only two of these functions are constant and six are balanced. As representatives of these we present in Table III one constant and three balanced functions. The others are related by inverting the qubits.

The functions in Table III are implemented by the four unitary transformations $U_f \in \{U_{0000}, U_{0101}, U_{0011}, U_{0110}\}$ represented by diagonal matrices where the diagonal part is shown in Eq. (37)

$$U_{0000} = \{+1, +1, +1, +1\} = I_4,$$
(37)

$$U_{0101} = \{+1, -1, +1, -1\} = -ie^{i\pi I_{z2}},$$
(38)

$$U_{0011} = \{+1, +1, -1, -1\} = -ie^{i\pi I_{z1}},$$
(39)

$$U_{0110} = \{+1, -1, -1, +1\} = e^{i\pi(I_{z1}+I_{z2})}.$$
(40)

Note that these transformations are z rotations which we implemented by applying the corresponding phase rotations to the second Hadamard transformation.

B. The S-bus implementation

The two-qubit Deutsch algorithm can readily be implemented by applying the following pulse sequence:

$$U_{\text{Deutsch}} = U_{f(x)}^{\dagger} P_{y1,y2}(-\pi/2) U_{f(x)} P_{y1,y2}(\pi/2).$$
(41)

The two Hadamard transformations were replaced by $\pi/2$ pulses with inverse phase. The second pulse was phase rotated corresponding to the appropriate unitary transformation.

Although it is sufficient to evaluate just the states of the first bit in order to decide if the function is constant or balanced we have in addition performed a complete density matrix tomography in order to evaluate the performance of the implementation of the two qubit Deutsch algorithm. The MQE tomography of the density matrices after applying the Deutsch algorithm is included in Fig. 10.

The balanced function corresponds to the identity matrix and no change of the initial ρ_{00} state is expected. The appli-
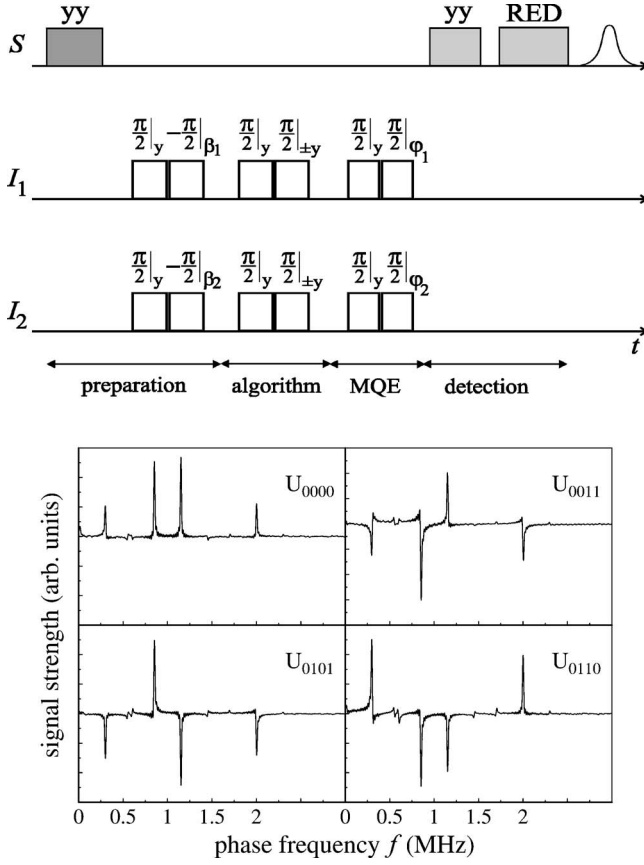
FIG. 10. Top: Pulse sequence for the implementation of the Deutsch algorithm. Bottom: Density matrix tomography after implementing all four functions defined in Table III.

cation of the three balanced functions converts the initial density matrix ρ_{00} into the residual pure density matrices ρ_{01}, ρ_{10}, and ρ_{11} as is seen in Fig. 10.

IX. ENTANGLED NUCLEAR SPINS

Entangled nuclear qubit states have been created by the standard selective Hadamard followed by the CNOT operation. The advantage for applying the S-bus concept compared with direct nuclear spin entanglement lies in the enormous increase in *polarization* mediated by the electron spin.

Consider as an example the $\Psi^{(-)}$ state which would be expressed in the S-bus concept as

$$\rho_\Psi = \frac{1}{8}I_3 - \Theta S_z \otimes \left(\frac{1}{4}I_2 - I_{x1}I_{x2} - I_{y1}I_{y2} - I_{z1}I_{z2} \right). \quad (42)$$

Applying the Prerez-Horodecki approach [36,37] of partial transpose (PT) one finds the quantum limit is reached for $\Theta > 1/2$. Note that $\Theta = \tanh(\hbar\omega_S/2k_BT)$ contains the electron Larmor frequency which is about 600 times larger that the nuclear Larmor frequency ω_I. Correspondingly the quantum limit can be reached at a much higher temperature as compared with direct nuclear entanglement.

X. SUMMARY AND OUTLOOK

We have introduced the S-bus concept of quantum computing which capitalizes on the distributed hyperfine couplings of nuclear spins (client qubits) to an electron spin (bus qubit). It was shown that this situation allows to prepare highly correlated qubit registers just by applying pulse sequences to the bus qubit. Quantum algorithms were implemented by unitary transformations on the client qubits and the result was read out by the bus qubit. There are several benefits of this procedure as compared with directly working with electron spins. First of all the decoherence times of nuclear spins in solids are appreciably longer than those of electron spins and can be enlarged by decoupling sequences beyond the ordinary T_2 relaxation [38]. Moreover the sensitivity of the qubit detection is enhanced by the indirect detection method due to the larger magnetic moment of the electron spin with the ratio of gyromagnetic moments γ_S/γ_I. Last but not least is the γ_S/γ_I ratio responsible for the much larger purity of the client qubit density matrix as compared with their original Boltzmann density matrix. The quantum critical regime can therefore be reached at a higher temperature/magnetic field ratio. The concept can be extended to interconnected S-bus systems by designing solid structures which allow controllable exchange coupling between different S-bus clusters.

APPENDIX A: SUBSPACE PREPARATION AND DETECTION

Generalizing the treatment in Sec. II we must consider that in general there will be more qubits available than actually used in a quantum algorithm. We therefore separate the qubits into working qubits of number n and residual qubits of number $N-n$

$$\Pi_{nN}^{(\pm)} = \prod_{k=n+1}^{N} e^{\pm i\tau a_k I_{zk}} \quad (A1)$$

with $\Pi_N^{(\pm)} = \Pi_n^{(\pm)}\Pi_{nN}^{(\pm)}$. This allows to treat the multiqubit registers present in the S-bus system consistently.

The preparation and detection of the qubit density matrix includes preparing for pseudopure density matrices followed by a quantum algorithm and a detection sequence. This is discussed in the following sections for three different preparation and detection sequences.

1. *yy* sequence

After a $P_y(\pi/2)$-τ-$P_y(\pi/2)$ sequence (Mims sequence [17]) the density matrix can be expressed as

$$\rho_{yy} = \frac{1}{2}(\Pi_n^{(+)}\Pi_{nN}^{(+)} + \Pi_n^{(-)}\Pi_{nN}^{(-)}) \tag{A2}$$

which translates readily into

$$\rho_{yy} = \frac{1}{2}\left(\prod_{j=1}^{n}(c_jI_2 + is_j2I_{zj})\right)\Pi_{nN}^{(+)} + \frac{1}{2}\left(\prod_{j=1}^{n}(c_jI_2 - is_j2I_{zj})\right)\Pi_{nN}^{(-)}. \tag{A3}$$

Single qubit algorithms are set up in such a way that finally only diagonal states are present which allows one to express the outcome to be presented by a scaling factor $-1 \leq S_j \leq 1$ in front of the I_{zj} operators. This results in the density matrix

$$\tilde{\rho}_{yy} = \frac{1}{2}\left(\prod_{j=1}^{n}(c_jI_2 + is_jS_j2I_{zj})\right)\Pi_{nN}^{(+)}$$
$$+ \frac{1}{2}\left(\prod_{j=1}^{n}(c_jI_2 - is_jS_j2I_{zj})\right)\Pi_{nN}^{(-)}. \tag{A4}$$

If the same sequence is used for detection the resulting signal can be expressed as

$$S_{yy} = \frac{1}{2^N}\text{Tr}\{\rho_{yy}\tilde{\rho}_{yy}\} \tag{A5}$$

which leads after performing the trace operation to

$$S_{yy} = \frac{1}{2}\left(\prod_{j=1}^{n}(c_j^2 + s_j^2S_j) + M_{N-n}\prod_{j=1}^{n}(c_j^2 - s_j^2S_j)\right) \tag{A6}$$

with

$$M_{N-n} = \frac{1}{2^{N-n}}\text{Tr}\{\Pi_{nN}^{(+)2}\} = \prod_{k=n+1}^{N}(c_k^2 - s_k^2). \tag{A7}$$

2. *yx* sequence

Proceeding in the same way as in the previous section we arrive at

$$\rho_{yx} = \frac{i}{2}(\Pi_n^{(+)}\Pi_{nN}^{(+)} - \Pi_n^{(-)}\Pi_{nN}^{(-)}) \tag{A8}$$

which translates readily into

$$\rho_{yx} = \frac{i}{2}\left(\prod_{j=1}^{n}(c_jI_2 + is_j2I_{zj})\right)\Pi_{nN}^{(+)} - \frac{i}{2}\left(\prod_{j=1}^{n}(c_jI_2 - is_j2I_{zj})\right)\Pi_{nN}^{(-)} \tag{A9}$$

and including the scaling factor S_j to

$$\tilde{\rho}_{yx} = \frac{i}{2}\left(\prod_{j=1}^{n}(c_jI_2 + is_jS_j2I_{zj})\right)\Pi_{nN}^{(+)}$$
$$- \frac{i}{2}\left(\prod_{j=1}^{n}(c_jI_2 - is_jS_j2I_{zj})\right)\Pi_{nN}^{(-)}. \tag{A10}$$

Using the same sequence for detection the resulting signal is defined as

$$S_{yx} = \frac{1}{2^N}\text{Tr}\{\rho_{yx}\tilde{\rho}_{yx}\} \tag{A11}$$

which leads after performing the trace operation to

$$S_{yx} = \frac{1}{2}\left(\prod_{j=1}^{n}(c_j^2 + s_j^2S_j) - M_{N-n}\prod_{j=1}^{n}(c_j^2 - s_j^2S_j)\right). \tag{A12}$$

It is not necessary, however, to use also a *yx* sequence for detection. Any other sequence might be used instead. The change in the expression (A12) can be readily calculated.

3. *y π4* sequence

Proceeding in the same way as in the previous section we arrive at

$$\rho_{y\pi4} = \frac{1+i}{2\sqrt{2}}\Pi_n^{(+)}\Pi_{nN}^{(+)} + \frac{1-i}{2\sqrt{2}}\Pi_n^{(-)}\Pi_{nN}^{(-)} \tag{A13}$$

which translates readily into

$$\rho_{y\pi4} = \frac{1+i}{2\sqrt{2}}\prod_{j=1}^{n}(c_jI_2 + is_j2I_{zj})\Pi_{nN}^{(+)}$$
$$+ \frac{1-i}{2\sqrt{2}}\prod_{j=1}^{n}(c_jI_2 - is_j2I_{zj})\Pi_{nN}^{(-)} \tag{A14}$$

and including the scaling factor S_j to

$$\tilde{\rho}_{y\pi4} = \frac{1+i}{2\sqrt{2}}\prod_{j=1}^{n}(c_jI_2 + is_jS_j2I_{zj})\Pi_{nN}^{(+)}$$
$$+ \frac{1-i}{2\sqrt{2}}\left(\prod_{j=1}^{n}(c_jI_2 - is_jS_j2I_{zj})\right)\Pi_{nN}^{(-)}. \tag{A15}$$

With the same sequence for detection the observed signal is defined as

$$S_{y\pi4} = \frac{1}{2^N}\text{Tr}\{\rho_{y\pi4}\tilde{\rho}_{y\pi4}\} \tag{A16}$$

and one obtains after performing the trace operation

$$S_{y\pi4} = \frac{1}{2}\prod_{j=1}^{n}(c_j^2 + s_j^2S_j). \tag{A17}$$

4. Total density matrices

In summary the density matrices derived in the previous sections can in general be expressed as

$$\rho_I = \frac{1}{2^N}p_0I_0 + \frac{1}{2^{N-1}}\sum_j p_jI_{zj}$$
$$+ \frac{1}{2^{N-2}}\sum_{j<k}p_{jk}I_{zj}I_{zk} + \cdots + p_{1,\dots,N}\prod_j^N I_{zj}, \tag{A18}$$

where the parameters p_q, etc., depend on products of the parameter c_j and s_j. Comparing with Eqs. (14), (18), and (22)

we find the following relation between the p_q and the c_j and s_j products

$$p_q = 2^N \prod_{j \in \{q\}} s_j \prod_{k \in \{N-q\}} c_k, \tag{A19}$$

where q labels the set of s_j products. Note that pure states correspond to all $|p_q|$ equal and in particular equal to one. This is achieved in the special case $s_j = c_k = 1/\sqrt{2}$. The detection signal involving ρ_I according to Eq. (A18) can be expressed as $\text{Tr}(\rho_I \tilde{\rho}_I)$ and leads to

$$S_D = \frac{1}{2^N} \left(p_0^2 + \sum_j^N S_j p_j^2 + \sum_{j<k} S_j S_k p_{jk}^2 + \sum_{j<k<q} S_j S_k S_q p_{jkq}^2 \right.$$

$$\left. + \cdots + p_{1,\ldots,N}^2 \prod_j^N S_j \right) \tag{A20}$$

and alternatively in terms of the c_j and s_j parameters to

$$S_D = \prod_j^N c_j^2 + \sum_j^N S_j s_j^2 \prod_{k \neq j} c_k^2 + \sum_{j<k} S_j S_k s_j^2 s_k^2 \prod_{q \neq j,k} c_q^2$$

$$+ \sum_{j<k<m} S_j S_k S_m s_j^2 s_k^2 s_m^2 \prod_{q \neq j,k,m} c_q^2 + \cdots + \prod_j^N S_j s_j^2. \tag{A21}$$

APPENDIX B: TRIPLE ENDOR

The distinction which ENDOR line belongs to which $m_S = \pm 1/2$ sublevel system is usually made by so-called Triple-ENDOR where one ENDOR line is saturated while all other ENDOR lines are consecutively excited. Only those ENDOR lines which are affected by the saturation belong to the same m_S sublevel system.

Applying Eq. (24a) for $n=2$ results in

$$S_{yy}^{(2)} = \frac{1}{2}(c_{j1}^2 + S_{j1}s_{j1}^2)(c_{j2}^2 + S_{j2}s_{j2}^2)$$

$$+ \frac{1}{2}(c_{j1}^2 - S_{j1}s_{j1}^2)(c_{j2}^2 - S_{j2}s_{j2}^2)M_{N-2}. \tag{B1}$$

A typical TRIPLE experiment consists of saturating the line of I_{j1} ($S_{j1}=0$) and sweeping through any of the other lines of I_{j2} and changing their state by S_{j2}. If we define the TRIPLE experiment in the same way as we did in the ENDOR experiment as the difference between the signal with no irradiation at the line of I_{j2} ($S_{j2}=1$) and irradiation with strength S_{j2} we obtain

$$S_{\text{TRIPLE}} = (1 - S_{j2})c_{j1}^2 s_{j2}^2 P_2^{(-)}. \tag{B2}$$

In other words all those residual ENDOR lines which belong to the same m_S sublevel system are attenuated by the factor c_{j1}^2. This allows one to determine this parameter for all ENDOR lines successively. The ratio of attenuation with respect to the ENDOR line is given by

$$R_T = c_{j1}^2 \frac{P_1^{(-)}}{P_2^{(-)}} \tag{B3}$$

which essentially corresponds to c_{j1}^2 since in many cases $P_1^{(-)} \simeq P_2^{(-)}$.

[1] D. G. Cory, A. F. Fahmy, and T. F. Havel, Proc. Natl. Acad. Sci. U.S.A. **94**, 1634 (1997).

[2] J. A. Jones and M. Mosca, J. Chem. Phys. **109**, 1648 (1998).

[3] I. L. Chuang, L. M. K. Vandersypen, X. Zhou, D. W. Leung, and S. Lloyd, Nature (London) **393**, 143 (1998).

[4] I. L. Chuang, N. Gershenfeld, and M. Kubinec, Phys. Rev. Lett. **80**, 3408 (1998).

[5] J. A. Jones, M. Mosca, and R. H. Hansen, Nature (London) **393**, 344 (1998).

[6] L. M. K. Vandersypen, M. Steffen, G. Breyta, C. S. Yannoni, M. H. Sherwood, and I. L. Chuang, Nature (London) **414**, 883 (2001).

[7] D. G. Cory, M. D. Price, and T. F. Havel, Physica D **120**, 82 (1998).

[8] E. Knill, I. Chuang, and R. Laflamme, Phys. Rev. A **57**, 3348 (1998).

[9] W. S. Warren, N. Gershenfeld, and I. Chuang, Science **277**, 1688 (1997).

[10] S. L. Braunstein, C. M. Caves, R. Jozsa, N. Linden, S. Popescu, and R. Schack, Phys. Rev. Lett. **83**, 1054 (1999).

[11] E. Knill and R. Laflamme, Phys. Rev. Lett. **81**, 5672 (1998).

[12] B. E. Kane, Nature (London) **393**, 133 (1998).

[13] D. Loss and D. P. Di Vincenzo, Phys. Rev. A **57**, 120 (1998).

[14] J. M. Kikkawa and D. D. Awschalom, Phys. Rev. Lett. **80**, 4313 (1998).

[15] A. V. Khaetskii, D. Loss, and L. Glazman, Phys. Rev. Lett. **88**, 186802 (2002).

[16] E. Abe, K. M. Itoh, J. Isoya, and S. Yamasaki, Phys. Rev. B **70**, 033204 (2004).

[17] W. B. Mims, Proc. R. Soc. London **283**, 452 (1965).

[18] M. Mehring, P. Höfer, H. Käß, and A. Grupp, Europhys. Lett. **6**, 463 (1988).

[19] G. Drobny, A. Pines, S. Sinton, D. Weitekamp, and D. Wemmer, Faraday Symp. Chem. Soc. **13**, 49 (1979).

[20] D. Weitekamp, J. Garbow, and A. Pines, J. Chem. Phys. **77**, 2870 (1982).

[21] J. Baum, M. Munowitz, A. N. Garroway, and A. Pines, J. Chem. Phys. **83**, 2015 (1985).

[22] J. Baum and A. Pines, J. Am. Chem. Soc. **108**, 7447 (1986).

[23] K. Saalwächter and H. W. Spiess, J. Chem. Phys. **114**, 5707 (2001).

[24] J. M. Baker, E. R. Davies, and J. P. Hurrel, Proc. R. Soc. London, Ser. A **308**, 403 (1968).

[25] J. Mende, Ph.D. thesis, Universität Stuttgart, Stuttgart, 2005.

[26] G. Bodenhausen, R. L. Vold, and R. G. Vold, J. Magn. Reson. (1969-1992) **37**, 93 (1980).

[27] J. Mende and M. Mehring (unpublished).

[28] H. G. Krojanski and D. Suter, Phys. Rev. Lett. **93**, 090501

(2004).

[29] G. A. Morris and R. Freeman, J. Am. Chem. Soc. **101**, 760 (1979).

[30] N. A. Gershenfeld and I. L. Chuang, Science **275**, 350 (1997).

[31] Arvind, K. Dorai, and A. Kumar, Pramana **56**, L705 (2001).

[32] J. Kim, J.-S. Lee, S. Lee, and C. Cheong, Phys. Rev. A **62**, 022312 (2000).

[33] D. Deutsch and R. Jozsa, Proc. R. Soc. London, Ser. A **439**, 553 (1992).

[34] R. Cleve, A. Ekert, C. Macchiavello, and M. Mosca, Proc. R. Soc. London, Ser. A **454**, 339 (1998).

[35] D. Collins, K. W. Kim, and W. C. Holton, Phys. Rev. A **58**, R1633 (1998).

[36] A. Peres, Phys. Rev. Lett. **77**, 1413 (1996).

[37] M. Horodecki, P. Horodecki, and R. Horodecki, Phys. Lett. A **223**, 1 (1996).

[38] A. Heidebrecht, J. Mende, and M. Mehring, Solid State Nucl. Magn. Reson. **29**, 90 (2006).